AIMS Mathematics, 10(8): 18295–18320.
DOI:10.3934/math.2025817
Received: 04 June 2025
Revised: 28 July 2025
Accepted: 06 August 2025
Published: 13 August 2025

https://www.aimspress.com/journal/Math

Research article

A discrete-time mathematical model for mosaic disease dynamics in cassava: Neimark-Sacker bifurcation and sensitivity analysis

Selim Reja[1,*], **Fahad Al Basir**[2,*] **and Khalid Aldawsari**[3]

[1] Agricultural and Ecological Research Unit, Indian Statistical Institute, Kolkata 700108, West Bengal, India

[2] Department of Mathematics, Asansol Girls' College, Asansol 713304, West Bengal, India

[3] Department of Mathematics, College of Science and Humanities, Prince Sattam Bin Abdulaziz University, Al Kharj 11942, Saudi Arabia

* **Correspondence:** Email: selimreja06@gmail.com, fahadbasir@gmail.com.

Abstract: Cassava mosaic disease remains a significant threat to cassava production, leading to severe yield losses and food insecurity. While several continuous-time models have been proposed to understand cassava mosaic disease transmission, there is limited understanding of cassava mosaic disease behavior in discrete-time settings. Discrete-time models are often easier to apply in agricultural settings, as they align more naturally with seasonal planting schedules and data collection intervals. To address this, we developed and analyzed a novel discrete-time mathematical model that captured the complex dynamics of cassava mosaic disease transmission via whitefly vectors. We introduced a density-dependent modification theorem for the nonnegativity and discussed the boundedness of solutions. The basic reproduction number was derived, and the stability of the disease-free equilibrium was examined. Additionally, we investigated the existence and stability of endemic fixed points. We conducted an analytical study of the Neimark-Sacker bifurcation using a novel approach without eigenvalues. Furthermore, we performed a comprehensive sensitivity analysis of our discrete model using Sobol indices. Numerical simulations validated our analytical findings and illustrated the impact of various parameters on the stability of fixed points. We also presented stability regions in different parameter planes. Our findings emphasized that elevated infection rates contributed to seasonal outbreaks of cassava mosaic disease. Furthermore, effective management of both plant infection rates and vector abundance was essential for controlling the disease. Finally, our results were consistent with those obtained from continuous models.

Keywords: discrete model setup; boundedness and convergence of solutions; Jury criteria; Sobol indices and sensitivity analysis; Neimark-Sacker bifurcation; numerical verifications
Mathematics Subject Classification: 39A22, 39A28, 39A30

1. Introduction

Cassava is a vital staple crop for millions of people, particularly in tropical and subtropical regions. It is a major source of carbohydrates and plays a crucial role in food security [1]. However, mosaic disease significantly threatens cassava production, a devastating viral disease primarily transmitted by the whitefly. It leads to a reduction in cassava productivity by up to 80% in some cases [2]. This disease is caused by Begomoviruses, belonging to the family Geminiviridae [3]. It is well known that discrete models are particularly helpful to plant biologists, as they often align more closely with the way biological and ecological data is collected, typically at specific time intervals rather than continuously. While continuous models provide valuable insights into disease dynamics, discrete-time models are especially advantageous for capturing the episodic nature of interventions and disease progression observed in real agricultural settings. Although a continuous counterpart of our model exists, our objective is not to draw a direct comparison between the discrete and continuous outcomes. Instead, our focus is on demonstrating that the results obtained from the discrete model are in alignment with those from the continuous framework, thereby reinforcing the reliability and applicability of our approach. Importantly, understanding the mechanisms of mosaic disease through a discrete theoretical modeling lens is essential for developing effective, practical disease management strategies. Such strategies can help mitigate the spread of infection and reduce associated economic losses, thereby supporting agricultural productivity and sustainability.

Whiteflies rank as the second most impactful vector of plant viruses, largely attributed to their capacity to transmit diverse pathogens, notably those belonging to the genus Begomoviruses, which encompasses around 200 distinct members [4]. Their interaction with cassava plants is intricate, as these insects serve as vectors and directly harm cassava leaves through feeding. As phloem-feeding insects, whiteflies acquire the virus while feeding on infected cassava plants and transmit it to healthy ones [5]. The resulting mosaic virus infection (*Begomoviruses*) manifests as speckled and discolored leaves. Mosaic disease symptoms include leaf chlorosis, mosaic patterns, leaf distortion, and stunted growth, which significantly reduce photosynthetic efficiency [6]. Whiteflies serve as the leading carriers for virus transmission, with infection rates rising as plants grow and develop quickly [7]. Plant density is a key factor influencing the spread of viruses [8]. While a single infected whitefly can transmit the virus, the risk escalates when multiple infected individuals feed on the same plant, leading to widespread outbreaks [9]. Beyond transmitting the virus, whiteflies actively damage plants by feeding on leaves and depleting their sap. Once established in a plantation, they can quickly spread to surrounding vegetation [10]. The virus needs a minimum of three hours of feeding to be acquired, followed by an eight-hour latent period before it can be transmitted. Visible symptoms typically appear within three to five weeks [11].

Models have become essential for studying the epidemiology of plant diseases, providing valuable insights into disease transmission dynamics [12]. These models enable researchers to predict potential outbreaks and assess the effectiveness of various intervention strategies. In particular, mathematical models have been extensively applied to study the spread of whitefly-borne mosaic disease in cassava. Several studies have explored different aspects of this disease. For instance, studies in [13, 14] have developed frameworks to model the spread of whitefly-borne mosaic disease in cassava. Additionally, a comprehensive model designed for cassava plantations was introduced in [15], offering a structured approach to understanding disease progression. Study [16] develops a stochastic model for cassava

mosaic disease using a continuous-time Markov chain derived from a deterministic framework. It reveals that disease extinction is more probable when the infection is introduced by vectors rather than by infected plants. By offering practical guidance for optimizing disease control without disrupting the distribution of healthy planting materials, study [17] evaluates the combined impact of trade restrictions and clean seed systems through mathematical modeling of cassava mosaic disease. Windbreaks and resistant cassava varieties are shown to be the most effective in reducing yield loss, according to [18], which models the spatial-temporal spread of African Cassava Mosaic Disease using ordinary differential equations (ODEs) and partial differential equations (PDEs) systems. Beyond cassava, similar modeling approaches have been employed to investigate whitefly-vectored mosaic disease in Jatropha plants. In [19], Venturino et al. derived a mathematical model to study the propagation dynamics of the mosaic disease in the *Jatropha curcas* plantation. Subsequently, Al Basir et al. [20] extended this model, incorporating the effects of control measures such as roguing and insecticide application to evaluate their impact on disease management.

Mathematical models for disease dynamics are traditionally formulated within continuous-time frameworks [21]. However, applying these models to real-life scenarios where data is typically collected at discrete intervals is challenging. In contrast, discrete-time models offer a more practical approach by aligning naturally with observational data and measurement frequencies [22–24]. Researchers have increasingly explored discrete-time epidemiological models for several key reasons. First, they are particularly effective in modeling plant disease control strategies, where interventions and observations occur at specific time points. Second, they serve as valuable tools for numerically approximating and analyzing continuous-time models, providing insights that may be difficult to obtain through purely analytical methods. Lastly, discrete-time frameworks can capture a diverse range of critical dynamic behaviors, including complex outbreak patterns and nonlinear interactions, which may be challenging to characterize using continuous models alone [25–28].

Discrete-time models provide valuable insights into the periodic outbreaks of diseases, enabling the evaluation of vector control strategies and the strategic deployment of resistant cassava varieties. However, despite their potential, discrete models for plant mosaic disease remain largely underexplored. The development and validation of such models could address critical gaps in epidemiological research and improve disease management in cassava-producing regions. With this in mind, we propose a discrete-time mathematical model, drawing inspiration from the continuous-time models established in [19, 20, 29]. Unlike recent research, such as the theta-logistic model introduced by Chowdhury et al. in [30], which focuses on whitefly-borne mosaic disease and examines the impacts of two biological control measures, the approach by Chowdhury et al. [30] has certain limitations. Specifically, it relies on numerical methods to study stability switches via bifurcation and lacks a robust theoretical foundation. Therefore, a more realistic discrete-time modeling approach is needed to enhance understanding of cassava mosaic disease dynamics before implementing effective control measures.

The Neimark-Sacker bifurcation, which describes the emergence of quasiperiodic dynamics via a torus bifurcation in discrete-time systems, is relevant to the Keller-Segel models of chemotaxis when discretized or when considering periodic forcing or modulation in parameters. Sensitivity analysis, often applied to investigate the dependence of model outcomes on parameter variations, can reveal the onset of such bifurcations in the Keller-Segel system, particularly under perturbations in chemotactic sensitivity or diffusivity. Thus, the interplay between bifurcation theory and sensitivity analysis

provides insight into the stability and transition dynamics of chemotactic pattern formation [31–33].

Sensitivity analysis assesses the influence of input variables on the output of a mathematical model, aiding in the identification of key parameters and system simplification [34]. The common methods available for determining the sensitivity of a parameter are local sensitivity analysis (small input variations), global sensitivity analysis (entire input range effects), Monte Carlo methods (random sampling-based uncertainty evaluation), and Sobol's method (variance-based quantification of input contributions). For cassava mosaic disease, sensitivity analysis helps to identify the key factors influencing the transmission and control of the disease [35]. In this research, we use Sobol's method to identify the significant parameters of the proposed discrete-time model.

Although cassava mosaic disease has been the subject of numerous studies, discrete-time modeling of its dynamics remains underexplored. Existing discrete models are limited in scope and fail to capture the disease's progression fully. To address this gap, we develop a novel discrete-time mathematical model that explicitly incorporates the role of the vector population in disease transmission. We first establish a density-dependent positivity theorem using the constant growth theorem, marking the first application of this approach in a discrete-time framework. We then analyze the stability of the fixed points. Given the lack of a standard simulation framework for identifying the most sensitive parameter in discrete-time models, we perform a global sensitivity analysis using the Sobol's index method to identify influential parameters. To investigate bifurcation behavior, we derive and numerically validate the conditions for a Neimark–Sacker bifurcation, demonstrating its occurrence in the model. Furthermore, we delineate the stability regions for key parameters to better understand their influence on system dynamics. This study endeavors to address these theoretical issues by analyzing a comprehensive set of scenarios that encapsulate the complex dynamics of cassava mosaic disease within a discrete modeling framework. Additionally, we validate our findings by comparing them with results from existing continuous models, and observe a strong alignment, reinforcing the robustness of our approach. The discrete setup holds particular significance as it not only simplifies implementation but also effectively captures the seasonality effects inherent in cassava mosaic disease transmission, making it a practical and insightful tool for real-world applications. The resulting insights hold significant promise for enriching the understanding of discrete models for mosaic diseases.

The remaining sections of this research article are organized as follows: Section 2 introduces the formulation of the mathematical model and its discrete representation. In Sections 3–5, we examine nonnegativity and boundedness, identify the fixed points, and establish their existence conditions and the basic reproduction number. Section 6 explores the local stability analysis of various fixed points. The bifurcation analysis is presented in Section 7, followed by numerical verification and results in Section 9. Finally, Section 10 discusses our findings and concludes the paper.

2. Derivation of the discrete-time model

Mathematical modeling is essential to understand and manage mosaic disease in cassava. Researchers can develop effective and sustainable solutions to protect cassava production around the world by integrating models with field data. The mosaic disease model has been studied throughout history using continuous-time models, but it is not difficult to integrate with real-world data when we consider discrete models that improve decision-making in the management of mosaic diseases. Keeping this in mind, we first discuss the continuous-time model and then represent that model in a

discrete sense.

For our modeling, we consider plant and vector populations. Here, we consider four key populations that interact over time. Let $x(t)$ represent susceptible cassava plants vulnerable to infection, while $y(t)$ denotes infected plants struggling under the grip of mosaic disease. In the realm of disease carriers, $u(t)$ represents susceptible whitefly vectors, not yet infected by the virus, while $v(t)$ captures infected whiteflies, actively spreading the disease. The growth of susceptible cassava plants follows a logistic pattern, limited by a carrying capacity k and driven by an intrinsic growth rate r. When an infected whitefly feeds on a healthy plant, the virus spreads, modeled by the mass action term λxv. In this context, λ signifies the effective rate of contact per capita between susceptible plants and infected vectors. Once infected, plants face a mortality rate m due to the impact of the disease. The whitefly growth rate is modeled using a logistic function, where b represents the intrinsic growth rate and a denotes the maximum vector abundance per plant. Since the maximum abundance of whiteflies depends on the cassava plant, we define the carrying capacity as $a(x + y)$. The term βuy represents the interaction between non-infective vectors and infected plants, where β is the interaction rate between non-infected vectors and infected plants, and $u(t)$ is the number of non-infected vectors. Additionally, μ represents the natural mortality rate of the vector.

Using the assumptions outlined above, we propose the following model:

$$\begin{aligned}
\frac{dx}{dt} &= rx\left[1 - \frac{x+y}{k}\right] - \lambda xv, \\
\frac{dy}{dt} &= \lambda xv - my, \\
\frac{du}{dt} &= b(u+v)\left[1 - \frac{u+v}{a(x+y)}\right] - \beta uy, \\
\frac{dv}{dt} &= \beta uy - \mu v.
\end{aligned} \tag{2.1}$$

Most species abundance data for the eco-epidemiological study are generally observed discretely. So, we represent the above continuous-time equation in a discrete setup. We employ the Euler discretization method for the model (2.1). Resultant revised model of the Eq (2.1) is:

$$\begin{aligned}
x_{t+1} - x_t &= rx_t\left[1 - \frac{x_t+y_t}{k}\right] - \lambda x_t v_t, \\
y_{t+1} - y_t &= \lambda x_t v_t - my_t, \\
u_{t+1} - u_t &= b(u_t+v_t)\left[1 - \frac{u_t+v_t}{a(x_t+y_t)}\right] - \beta u_t y_t, \\
v_{t+1} - v_t &= \beta u_t y_t - \mu v_t,
\end{aligned} \tag{2.2}$$

with initial conditions: $x_0 > 0,\ y_0 > 0,\ u_0 > 0,\ v_0 > 0$. The significance of the parameters are given in the Table 1.

Table 1. Description of parameters and their values [29].

Parameter	Short description	Value (unit)
r	intrinsic growth rate of cassava plants	0.1 day^{-1}
k	carrying capacity of cassava plants	100 m^{-2}
λ	rate of infection transmission from vector to plant	0.00025 vector^{-1} day^{-1}
b	reproduction rate of whitefly	0.5 day^{-1}
a	abundance of whitefly on a plants	5 plant^{-1}
β	rate of transmission of infection from plant to vector	0.0003 $\text{plant}^{-1}\text{day}^{-1}$
μ	natural mortality rate of whitefly	0.032 day^{-1}

3. Nonnegativity and boundedness

In discrete models, nonnegativity and boundedness are crucial in ensuring the models are realistic and meaningful. Nonnegativity constraint ensures that variables or parameters in the model cannot take negative values, and boundedness restricts variables to a specified range that reflects real-world constraints. In this section, we will prove that solutions of the discrete system (2.2) are nonnegative and bounded. [36] provides a theorem for nonnegativity. Here, we propose a modified version of this theorem considering density-dependent recruitment. Proof of this modified version can be easily done following the main theorem.

Theorem 1. *If the set of difference equations:*

$$\begin{aligned} y(n+1) =& \alpha y(n) + (1-\beta y(n))y(n) - \sum_{i=1}^{m} \psi_i(y(n+1))x_i(n+1), \quad n \geq 0 \\ x_1(n+1) =& (1-a_1)\, x_1(n) + \phi_1(y(n))x_L(n), \quad 1 \leq L \leq p \\ x_i(n+1) =& (1-a_i)\, x_i(n) + \phi_i(y(n))x_{i-1}(n), \quad i = 2,3,\ldots,p \end{aligned} \tag{3.1}$$

where $\psi_i(x), \phi_i(x) \in C^0(\mathbb{R}), 1 \leq i \leq p$, and $\phi_i, 1 \leq i \leq m$, and at least one of the $\psi_j (1 \leq j \leq L)$ is a strictly monotone increasing function and $y\psi_i(y) \geq 0,\ \forall y \in \mathbb{R}, i = 1,\ldots,p$ satisfy the following conditions:
(i) $\alpha > 0$;
(ii) $\beta < 1$;
(iii) $a_i < 1, i = 1,\ldots,p$;
(iv) $\phi_i(y)$ is not decreasing and $\phi_i(0) \geq 0, i = 1,\ldots,p$;
(v) $y\Psi_i(y) \geq 0, \forall y \in \mathbb{R}, i = 1,\ldots,p$;
(vi) $\exists$ s.t. $1 \leq \hat{\text{i}} \leq L$ and $\psi_{\hat{\text{i}}}$ is strictly increasing,
then all solutions of (3.1) are nonnegative, i.e., $y(n) > 0, x_i(n) > 0, n \geq 0, i = 1,\ldots,p$.

In our case, $p = 3, I = 2, L = 3, \psi_1(y) = \lambda y = \phi_1(y), \psi_2(y) = \frac{r}{K}y, \alpha = r, \beta = \frac{r}{K}, a_1 = m, a_2 = 0, a_3 = \mu, \phi_2(y) = 0, \phi_3(y) = 0$.

So, all conditions are satisfied for our model (2.2). Hence, solutions are nonnegative. This completes that all solutions of the model (2.2) are nonnegative.

Now, we establish the boundedness of solutions using the following theorem.

Theorem 2. *Any solution (x_t, y_t, u_t, v_t) of the discrete system (2.2) is bounded in the region D, where, $D = \{(x_t, y_t, u_t, v_t) : 0 \le x_t + y_t \le \frac{rK}{4m_0},\ 0 \le u_t + v_t \le \frac{barK}{16\mu m_0} + \eta_1\}$.*

Proof. Let $P_t = x_t + y_t$ and $Q_t = u_t + v_t$. Then, from the first two equations of the discrete system (2.2), we get

$$\begin{aligned} P_{t+1} - P_t &= rx_t\left[1 - \frac{P_t}{k}\right] - my_t \\ &= rP_t\left[1 - \frac{P_t}{k}\right] - my_t - rx_t \\ &\le \frac{rK}{4} - m_0 P_t, \quad \text{where, } m_0 = \min\{m, r\}. \end{aligned}$$

From this relation, we get, $\lim_{t\to\infty} \sup P_t \le \frac{rK}{4m_0}$.
Again, from the last two equations of the discrete system (2.2), we get

$$\begin{aligned} Q_{t+1} - Q_t &= bQ_t\left[1 - \frac{Q_t}{aP_t}\right] - \mu Q_t \\ &\le \frac{baP_t}{4} - \mu\left(Q_t - u_t\right) \\ &\le \frac{barK}{16m_0} + \mu\eta_1 - \mu Q_t. \end{aligned}$$

This relation gives: $\lim_{t\to\infty} \sup Q_t \le \frac{barK}{16\mu m_0} + \eta_1$, where $\eta_1 = \lim_{t\to\infty} u_t$.
This completes the proof. □

Thus, together with Theorems 1 and 2, we can say that the solutions of the discrete-time system (2.2) are nonnegative and bounded.

4. Fixed point analysis

In this section, we will find all possible fixed points for our system (2.2). For a fixed point in a discrete system, the value of the state variable remains the same at both time steps t and $(t + 1)$. Now, let $E(\bar{x}, \bar{y}, \bar{u}, \bar{v})$ be a system's (2.2) any arbitrary fixed point. Therefore, $x_{t+1} = x_t = \bar{x}$, $y_{t+1} = y_t = \bar{y}$, $u_{t+1} = u_t = \bar{u}$,$v_{t+1} = v_t = \bar{v}$. So, from (2.2), we get:

$$\begin{aligned} &\bar{x} + r\bar{x}\left[1 - \frac{\bar{x} + \bar{y}}{k}\right] - \lambda\bar{x}\bar{v} = \bar{x}, \\ &\bar{y} + \lambda\bar{x}\bar{v} - m\bar{y} = \bar{y}, \\ &\bar{u} + b(\bar{u} + \bar{v})\left[1 - \frac{\bar{u} + \bar{v}}{a(\bar{x} + \bar{y})}\right] - \beta\bar{u}\bar{y} = \bar{u}, \\ &\bar{v} + \beta\bar{u}\bar{y} - \mu\bar{v} = \bar{v}. \end{aligned}$$

After solving the above system, we get two biologically feasible fixed points of system (2.2), namely

(i) only cassava plant $E_1\,(k, 0, 0, 0)$, and
(ii) the disease-free point $E_0\,(k, 0, ak, 0)$, and

(iii) the endemic point, $E^*(x^*, y^*, u^*, v^*)$,

where

$$y^* = \frac{rx^*(k - x^*)}{rx^* + km}, \quad u^* = \frac{m\mu}{\beta\lambda x^*}, \quad v^* = \frac{rm(k - x^*)}{(rx^* + mk)\lambda},$$

and x^* satisfies the quartic equation

$$F(x) = a_4x^4 + a_3x^3 + a_2x^2 + a_1x + a_0 = 0, \tag{4.1}$$

where

$$\begin{aligned}
a_4 &= b\beta^2mr^2 + ab\beta^2k\lambda r^2 - a\beta^2k\lambda m\mu r - a\beta^2k\lambda\mu r^2 + abk\lambda mr,\\
a_3 &= -2b\beta m\mu r^2 - 2b\beta^2kmr^2 + a\beta^2k^2\lambda m\mu r - ab\beta^2k^2\lambda r^2 - ab\beta k\lambda m\mu r\\
&\quad + a\beta^2k^2\lambda\mu r^2 - ab\beta^2k^2\lambda mr - ab\beta k\lambda\mu r^2,\\
a_2 &= bm\mu^2r^2 - ab\beta k^2\lambda m^2\mu - ab\beta k^2\lambda m\mu r - 2b\beta km^2\mu r + b\beta^2k^2mr^2 + 2b\beta km\mu r^2,\\
a_1 &= 2bkm^2\mu^2r + 2b\beta k^2m^2\mu r > 0,\\
a_0 &= bk^2m^3\mu^2 > 0.
\end{aligned}$$

A positive root of (4.1) exists when either $a_4 < 0,\ a_3 > 0,\ a_2 > 0$ or $a_4 < 0,\ a_3 < 0, a_2 > 0$.

Remark 1. *To determine whether the point* $(0, 0, 0, 0)$ *qualifies as a steady state for the system, we need to address the singularity introduced by the denominator of the third equation of the system, which tends to zero as* $x + y \to 0$*. A potential resolution involves evaluating the limit of the righthand side as* $(x, y, u, v) \to (0, 0, 0, 0)$*. If this limit exists and equals* $(0, 0, 0, 0)$*, then the system may be continuously extended to the origin.*

Consider first the hyperplane defined by $u = v = 0$*, where* $x > 0$ *and* $y > 0$*. In this scenario, the third and fourth equations yield zero on the righthand side. Moreover, as* $x \to 0$ *and* $y \to 0$*, the righthand sides of the first two equations also approach zero. Thus, on this hyperplane, we observe that the limit* $\lim_{(x,y,u,v)\to(0,0,0,0)}(x, y, u, v)$ *equals* $(0, 0, 0, 0)$.

In contrast, when we examine the hyperplane $x = y = 0$ *with* $u > 0$ *and* $v > 0$*, the first two equations again yield zero. However, the third equation becomes problematic as it diverges to infinity, and maintains this behavior as* $u \to 0$ *and* $v \to 0$*. This divergence suggests that the limit does not exist, and, therefore, the origin* $(0, 0, 0, 0)$ *cannot be treated as a valid steady state of the system.*

5. Basic reproduction number

The basic reproduction number is a fundamental epidemiological measure that quantifies the average number of new infections caused by a single infected individual in a fully susceptible population. We use the next-generation matrix approach to find the basic reproduction number. This process is outlined for the continuous-time model by Driessche et al. and Hefferman et al. [37, 38]. Many authors use this method [39]. In our case, we used the next-generation matrix for discrete set-ups that are introduced by De Jong et al. [40].

Now, according to [41], we can write infective in the form:

$$X_0(t + 1) = G_0(X(t)),$$

where $X_0 = [y, v]^t$, and $G_0(X(t)) = \mathcal{F} + \mathcal{V}$. Here, $\mathcal{F}$ represents the vector of new infections that persist throughout the time interval, while $\mathcal{V}$ denotes the vector encompassing all other transitions. Therefore,

$$\mathcal{F} = \begin{pmatrix} \lambda x_t v_t \\ \beta u_t y_t \end{pmatrix}, \quad \mathcal{V} = \begin{pmatrix} (1-m)y_t \\ (1-\mu)v_t \end{pmatrix}.$$

So, two matrices F and V at disease-free equilibrium $E_0\,(k, 0, ak, 0)$ are:

$$F = \begin{pmatrix} 0 & \lambda k \\ \beta a k & 0 \end{pmatrix}, \; V = \begin{pmatrix} 1-m & 0 \\ 0 & 1-\mu \end{pmatrix}.$$

Now, the basic reproduction number is:

$$\mathcal{R}_0 = \rho\left(F[\mathbb{I} - V]^{-1}\right),$$

where ρ is the spectral radius of $F[\mathbb{I} - V]^{-1}$. Therefore, the resultant basic reproduction number is:

$$\mathcal{R}_0 = k\sqrt{\frac{\lambda\beta a}{m\mu}}. \tag{5.1}$$

6. Stability analysis

Stability analysis in discrete models captures disease dynamics in systems with natural time intervals. It helps us understand how infections evolve over successive steps. We must find the Jacobian matrix to achieve stability in our case.

Therefore, the Jacobian matrix at $E(x, y, u, v)$ of the system is given by:

$$J(E) = \begin{bmatrix} 1 + r\left(1 - \frac{2x+y}{k}\right) - \lambda v & -\frac{rx}{k} & 0 & -\lambda x \\ \lambda v & 1-m & 0 & \lambda x \\ \frac{b(u+v)^2}{a(x+y)^2} & \frac{b(u+v)^2}{a(x+y)^2} - \beta u & J_{33} & J_{34} \\ 0 & \beta u & \beta y & 1-\mu \end{bmatrix},$$

where

$$J_{33} = 1 + b\left[1 - \frac{2(u+v)}{a(x+y)}\right] - \beta y, \quad \text{and} \quad J_{34} = b\left[1 - \frac{2(u+v)}{a(x+y)}\right].$$

For stability of the fixed point E, we have to show that the eigenvalues corresponding to the Jacobian matrix are modulus less than 1. In other words, if $\rho_i,\ i = 1, 2, 3, 4$ are the eigenvalues at E, then the stability of E requires $|\rho_i| < 1,\ i = 1, 2, 3, 4$.

Now, we check the stability of our biologically feasible fixed points.

6.1. Stability of cassava plant-only-fixed point E_1

The Jacobian matrix at only cassava plant points $E_1\,(k, 0, 0, 0)$ of the system is given by:

$$J(E_1) = \begin{bmatrix} 1-r & -r & 0 & -\lambda k \\ 0 & 1-m & 0 & \lambda k \\ 0 & 0 & 1+b & -b \\ 0 & 0 & 0 & 1-\mu \end{bmatrix}.$$

The four eigenvalues of the Jacobian matrix at E_1 are $\rho_1 = 1 - m$, $\rho_2 = 1 - b\mu$, $\rho_3 = 1 - r$, and $\rho_4 = 1 + b$. The eigenvalue ρ_4 implies that for stability, b must be less than 0, which is not feasible. So, E_1 is always unstable.

6.2. Stability of disease-free fixed point E_0

The Jacobian matrix at the disease-free fixed points $E_0\,(k, 0, ak, 0)$ of the our system is

$$J(E_0) = \begin{bmatrix} 1-r & -r & 0 & -\lambda k \\ 0 & 1-m & 0 & \lambda k \\ ab & ab-\beta ak & 1-b & -b \\ 0 & \beta ak & 0 & 1-\mu \end{bmatrix}.$$

At the fixed point E_0, Jacobian matrix has two eigenvalues, namely, $\rho_1 = 1 - r$ and $\rho_2 = 1 - b$, and remaining eigenvalues satisfy the following equation:

$$f(\rho) = \rho^2 + l_1\rho + l_2 = 0, \tag{6.1}$$

where, $l_1 = 2(1 - m)$ and $l_2 = 1 + \frac{3}{4}m^2 + \frac{m}{2}(\mu - 4) - ak^2\beta\lambda$.

Two eigenvalues of the Jacobian matrix at E_0 are $\rho_1 = 1 - r$ and $\rho_2 = 1 - b$. Thus, $|\rho_1| < 1$ implies $r < 2$ and $\rho_2 = 1 - b$ implies $b < 2$.

Using the jury conditions from [42,43], we present the following lemma, which aids in deriving the remaining stability conditions based on the other two eigenvalues.

Lemma 1. *Let $P(\xi) = \xi^2 + l_1\xi + l_2 = 0$, and let ξ_1 and ξ_2 be its two roots. Then, $|\xi_1| < 1$ and $|\xi_2| < 1$ if $P(1) > 0$, $P(-1) > 0$, and $|l_2| < 1$.*

Using the above lemma, $|\xi_1| < 1$ and $|\xi_2| < 1$ if $1 + l_1 + l_2 > 0$, $1 - l_1 + l_2 > 0$, and $|l_2| < 1$.

From (6.1), we get

$$i. \quad 1 + l_1 + l_2 = 4 + \frac{3}{4}m^2 - 4m + m\mu(\frac{1}{2} - \mathcal{R}_0^2) > 0,$$

$$ii. \quad 1 - l_1 + l_2 = \frac{3}{4}m^2 + m\mu(\frac{1}{2} - \mathcal{R}_0^2) > 0, \text{ and}$$

$$iii. \quad |l_2| = |1 - 2m + \frac{3}{4}m^2 + m\mu(\frac{1}{2} - \mathcal{R}_0^2)| < 1.$$

These three conditions hold if $\mathcal{R}_0 < 1$. Therefore, the following theorem regarding the stability of E_0 can be established.

Theorem 3. *Our system is asymptotically stable at disease-free fixed points if $r < 2$, $b < 2$, and $\mathcal{R}_0 < 1$.*

6.3. Stability of endemic fixed point E^*

The Jacobian matrix at endemic fixed points $E^*(x^*, y^*, u^*, v^*)$ of the our system is given by:

$$J(E^*) = \begin{bmatrix} J_{11}^* & -\frac{rx^*}{k} & 0 & -\lambda x^* \\ \lambda v^* & 1-m & 0 & \lambda x^* \\ J_{31}^* & J_{32}^* & J_{33}^* & J_{34}^* \\ 0 & \beta u^* & \beta y^* & 1-\mu \end{bmatrix},$$

where

$$\begin{aligned} J_{11}^* &= 1 + r\left(1 - \frac{2x^* + y^*}{k}\right) - \lambda v^*, \quad J_{12}^* = -\frac{rx^*}{k}, \quad J_{14}^* = -\lambda x^*, \\ J_{21}^* &= \lambda v^*, \quad J_{22}^* = 1 - m, \quad J_{24}^* = \lambda x^*, \quad J_{31}^* = \frac{b(u^* + v^*)^2}{a(x^* + y^*)^2}, \\ J_{32}^* &= \frac{b(u^* + v^*)^2}{a(x^* + y^*)^2} - \beta u^*, \quad J_{33}^* = 1 + b\left[1 - \frac{2(u^* + v^*)}{a(x^* + y^*)}\right] - \beta y^*, \\ J_{34}^* &= b\left[1 - \frac{2(u^* + v^*)}{a(x^* + y^*)}\right], \quad J_{41}^* = \beta u^*, \quad J_{42}^* = \beta y^*, \quad J_{44}^* = 1 - \mu. \end{aligned}$$

The characteristic equation is,

$$\rho^4 + \sigma_1\rho^3 + \sigma_2\rho^2 + \sigma_3\rho + \sigma_4 = 0, \tag{6.2}$$

where

$$\begin{aligned} \sigma_1 &= -(J_{22}^* + J_{33}^* + J_{44}^* + J_{11}^*), \\ \sigma_2 &= J_{11}^*J_{22}^* - J_{12}^*J_{21}^* + J_{11}^*J_{33}^* + J_{11}^*J_{44}^* + J_{22}^*J_{33}^* + J_{22}^*J_{44}^* - J_{24}^*J_{42}^* + J_{33}^*J_{44}^* - J_{34}^*J_{43}^*, \\ \sigma_3 &= J_{12}^*J_{21}^*J_{33}^* + J_{11}^*J_{24}^*J_{42}^* + J_{12}^*J_{21}^*J_{44}^* - J_{11}^*J_{22}^*J_{33}^* - J_{11}^*J_{22}^*J_{44}^* - J_{14}^*J_{21}^*J_{42}^* - J_{11}^*J_{33}^*J_{44}^* \\ &\quad + J_{11}^*J_{34}^*J_{43}^* - J_{14}^*J_{31}^*J_{43}^* - J_{22}^*J_{33}^*J_{44}^* + J_{22}^*J_{34}^*J_{43}^* - J_{24}^*J_{32}^*J_{43}^* + J_{24}^*J_{33}^*J_{42}^*, \\ \sigma_4 &= \det(J(E^*)) = J_{11}^*J_{22}^*J_{33}^*J_{44}^* - J_{11}^*J_{22}^*J_{34}^*J_{43}^* + J_{11}^*J_{24}^*J_{32}^*J_{43}^* - J_{11}^*J_{24}^*J_{33}^*J_{42}^* - J_{12}^*J_{21}^*J_{33}^*J_{44}^* \\ &\quad + J_{12}^*J_{21}^*J_{34}^*J_{43}^* - J_{12}^*J_{24}^*J_{31}^*J_{43}^* - J_{14}^*J_{21}^*J_{32}^*J_{43}^* + J_{14}^*J_{21}^*J_{33}^*J_{42}^* + J_{14}^*J_{22}^*J_{31}^*J_{43}^*. \end{aligned}$$

Lemma 2. *Let ρ_i for $i = 1, 2, 3, 4$ be the roots of* (6.2)*. The conditions $|\rho_1| < 1$, $|\rho_2| < 1$, $|\rho_3| < 1$, and $|\rho_4| < 1$ hold if the following criteria, based on the Jury stability criterion [42, 43], are met.*

i) $|\sigma_4| < 1$,
ii) $1 + \sigma_1 + \sigma_2 + \sigma_3 + \sigma_4 > 0$,
iii) $1 - \sigma_1 + \sigma_2 - \sigma_3 + \sigma_4 > 0$,
iv) $|B_3| > |B_0|, \ |C_2| > |C_0|$,

where

$$|B_i| = \begin{vmatrix} \sigma_4 & \sigma_{3-i} \\ \sigma_0 & \sigma_{i+1} \end{vmatrix}, \quad |C_j| = \begin{vmatrix} B_3 & B_{2-j} \\ B_0 & B_{i+1} \end{vmatrix}$$

with $\sigma_0 = 1$, $i = 0,\ 3$, and $j = 0,\ 2$.

Hence, the following theorem is established regarding the stability of E^*.

Theorem 4. *The endemic equilibrium E^* is asymptotically stable if the conditions given in* (6.3) *are fulfilled.*

7. Bifurcation analysis

Due to their complex behaviors, bifurcation in discrete dynamical systems has garnered significant attention in recent research. This section explores the parametric conditions under which Neimark-Sacker bifurcation occurs for the endemic fixed point E^* of the system (2.2).

7.1. Neimark-Sacker bifurcation

In this subsection, we explore the Neimark-Sacker Bifurcation without finding the eigenvalues with the help of the two following articles [44, 45].

Lemma 3. *Let $\lambda \in \mathbb{R}$ be a bifurcation parameter of an n-dimensional discrete dynamical system $X_{t+1} = f_\lambda(X_t)$ and X^* be a fixed point. The characteristic polynomial corresponding to the Jacobian matrix $J(X^*) = \left(\sigma_{ij}\right)_{n\times n}$ of n-dimensional map $f_\lambda(X_t)$ is expressed as:*

$$P_\lambda(\rho) = \rho^n + \sigma_1\rho^{n-1} + \cdots + \sigma_{n-1}\rho + \sigma_n,$$

where $\sigma_i = \sigma_i(\lambda, c), i = 1, 2, 3, \ldots, n$, and the parameter c serves as a control variable or a parameter that needs to be determined. Let $\Delta_o^{\pm}(\lambda, c) = 1, \Delta_1^{\pm}(\lambda, c), \ldots, \Delta_n^{\pm}(\lambda, c)$ be a sequence of determinants defined by $\Delta_i^{\pm}(\lambda, c) = \det(M_1 \pm M_2)$, $i = 1, 2, 3, \ldots, n$, and the values of M_1 and M_2 given below:

$$M_1 = \begin{bmatrix} 1 & \sigma_1 & \sigma_2 & \ldots & \sigma_{i-1} \\ 0 & 1 & \sigma_1 & \ldots & \sigma_{i-2} \\ 0 & 0 & 1 & \ldots & \sigma_{i-3} \\ \ldots & \ldots & \ldots & \ldots & \ldots \\ 0 & 0 & 0 & \ldots & 1 \end{bmatrix} \text{ and } M_2 = \begin{bmatrix} \sigma_{n-i+1} & \sigma_{n-i+2} & \ldots & \sigma_{n-1} & \sigma_n \\ \sigma_{n-i+2} & \sigma_{n-i+3} & \ldots & \sigma_n & 0 \\ \ldots & \ldots & \ldots & \ldots & \ldots \\ \sigma_{n-1} & \sigma_n & \ldots & 0 & 0 \\ \sigma_n & 0 & \ldots & 0 & 0 \end{bmatrix}.$$

Moreover, the conditions mentioned below are also satisfied:

H1. Eigenvalue assignment: $\Delta_{n-1}^{-}(\lambda^*, c) = 0$, $\Delta_{n-1}^{+}(\lambda^*, c) > 0$, $P_{\lambda^*}(1) > 0$, $(-1)^n P_{\lambda^*}(-1) > 0$, $\Delta_i^{\pm}(\lambda^*, c) > 0, i = n-3, n-5, 1$ (or 2), when n is even or odd, respectively.

H2. Transversality condition: $\left[\frac{\mathrm{d}\left(\Delta_{n-1}^{-}(\lambda,c)\right)}{\mathrm{d}\lambda}\right]_{\lambda=\lambda^*} \neq 0$.

H3. Non-resonance condition: $\cos(2\pi/m) \neq \psi$, or resonance condition $\cos(2\pi/m) = \psi$, where $m = 3, 4, 5, \ldots$, and $\psi = -1 + 0.5P_{\lambda^*}(1)\Delta^-_{n-3}(\lambda, c) / \Delta^+_{n-2}(\lambda, c)$. Then, Neimark-Sacker Bifurcation (NSB) occurs at λ^*.

These conditions indicate that the system (2.2) undergoes Neimark-Sacker bifurcation where λ^* is the bifurcation parameter.

Theorem 5. *The fixed point E^* of the discrete dynamical system undergoes a Neimark-Sacker bifurcation at $\lambda = \lambda^*$ if the following conditions are satisfied:*

$$\begin{cases} 1 \pm \sigma_4 > 0, \\ 1 - \sigma_4 - \sigma_2 - \sigma_3^2 + \sigma_4^3 - \sigma_4^2(1 + \sigma_2) - \sigma_1^2\sigma_4 \\ \quad +2\sigma_2\sigma_4 + \sigma_1\sigma_3(1 + \sigma_4) = 0, \\ 1 + \sigma_4 + \sigma_2 - \sigma_3^2 - \sigma_4^3 - \sigma_4^2 + \sigma_1^2\sigma_4 - \sigma_2\sigma_4^2 \\ \quad -\sigma_1\sigma_3(1 - \sigma_4) > 0, \\ 1 + \sigma_1 + \sigma_2 + \sigma_3 + \sigma_4 > 0, \\ 1 - \sigma_1 + \sigma_2 - \sigma_3 + \sigma_4 > 0, \end{cases}$$

where $\sigma_1, \sigma_2, \sigma_3$, and σ_4 are the coefficient of the characteristic Eq (6.2).

Proof. From the above Lemma 3, in our case, $n = 4$, and the characteristic polynomial of our discrete system (2.2) calculated at $E^* = (x^*, y^*, u^*, v^*)$ given in (6.2), then we obtain:

$$\begin{cases} \Delta^{\pm}_1(\lambda) = 1 \pm \sigma_4 > 0, \\ \Delta^-_3(\lambda) = 1 - \sigma_4 - \sigma_2 - \sigma_3^2 + \sigma_4^3 - \sigma_4^2(1 + \sigma_2) \\ \quad -\sigma_1^2\sigma_4 + 2\sigma_2\sigma_4 + \sigma_1\sigma_3(1 + \sigma_4) = 0, \\ \Delta^+_3(\lambda) = 1 + \sigma_4 + \sigma_2 - \sigma_3^2 - \sigma_4^3 - \sigma_4^2 \\ \quad +\sigma_1^2\sigma_4 - \sigma_2\sigma_4^2 - \sigma_1\sigma_3(1 - \sigma_4) > 0, \\ P_\lambda(1) = 1 + \sigma_1 + \sigma_2 + \sigma_3 + \sigma_4 > 0, \\ (-1)^4 P_\lambda(-1) = 1 - \sigma_1 + \sigma_2 - \sigma_3 + \sigma_4 > 0. \end{cases}$$

□

Remark 2. *The value of λ^* at which system (2.2) undergoes Neimark-Sacker bifurcation occurs can be obtained by solving the equation $\Delta^-_3(\lambda) = 0$.*

Remark 3. *The above theorem is proposed on the parameter λ, but similar conditions can be established for the parameters a and β.*

8. Global sensitivity analysis

Understanding the primary drivers of plant disease spread is crucial [46]. To address this challenge, we employ global sensitivity analysis for our discrete disease model in cassava. Global sensitivity analysis in a simulation model evaluates how much each input parameter contributes to the overall variability of the output, allowing for the ranking of parameters based on their influence on model outcomes [47]. It helps identify which parameters significantly influence model outcomes, guiding efforts in understanding and accurately estimating those critical parameters. Several ways exist to

perform global sensitivity analysis, but most are suitable for continuous time models [48]. Here, we use Sobol's method for global sensitivity analysis as it can also be usable in discrete setups. This variance-based technique quantifies the contribution of individual or combined parameters to the output variability of a nonlinear model [49]. Sobol's sensitivity indices measure the proportion of variance attributed to a single parameter or interactions within a subset of parameters relative to the total variance. Typically, two types of Sobol's indices are computed: the first-order index, which represents the direct impact of an individual parameter, and the total effect index, which accounts for both direct and interaction effects [50]. First-order indices were estimated using the Sobol–Saltelli method, while total indices were determined using the Sobol–Jansen method. These approaches were selected based on their effectiveness in accurately estimating small first-order and large and small total indices.

We have conducted Sobol's sensitivity analysis for our model concerning the model's parameters using a 10, 000 sample size. Parameters are selected from feasible ranges to generate Latin hypercube sampling (LHS) for our analysis. The global sensitivity analysis results using Sobol's method are shown in Figure 1. The infection rates (λ, β), death rates (m, μ), and the abundance rate of vectors on plants (a) exhibit the highest first-order indices, indicating that these parameters alone significantly influence the system's response. Additionally, the total indices for these parameters exceed their first-order indices, suggesting that their influence increases when interacting with other factors. The remaining parameters, r, k, and b, also have first-order indices, but their impact is comparatively lower. Their total-order indices are also lower, implying that these parameters are less influential when dependent on other factors.

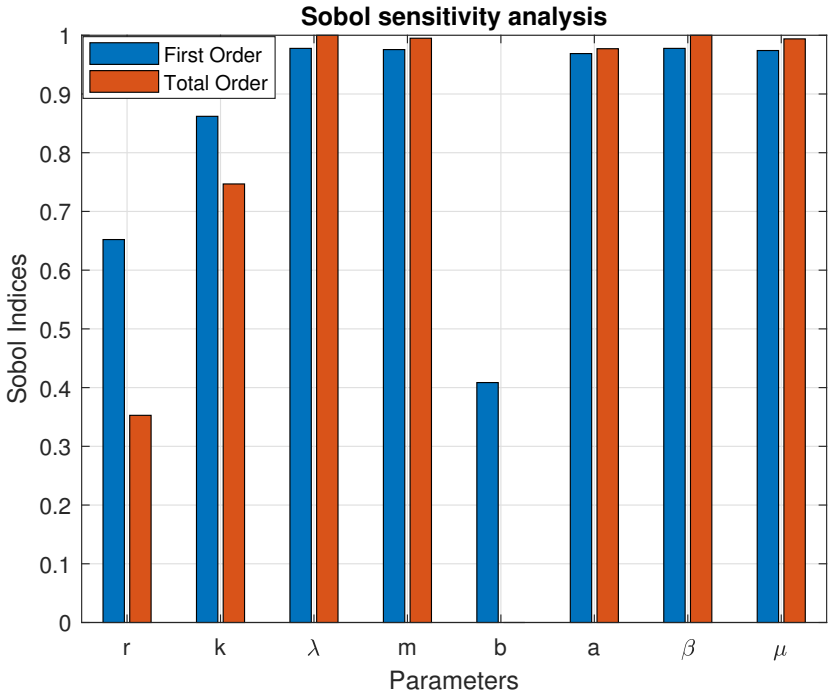

Figure 1. First and total order Sobol sensitivity indices of model parameters with respect to the system.

9. Numerical verification and results

Numerical verification is essential for discrete disease models to ensure accuracy, stability, and reliability. Numerical verification prevents incorrect conclusions by detecting errors in discretization, coding, or implementation. Here, we present the numerical results to validate the analytical findings discussed earlier for the system (2.2). The discrete formulation of the model (2.2) is numerically solved using the Forward Euler Scheme [27] in MATLAB.

To verify the convergence of the solution, we first plot the time series of the continuous model (2.1) using the parameter values from Table 1. For the discrete setup, model (2.2) is considered with a step length of 1. Its time series solution converges to the same equilibrium point as that of the continuous model. To further verify convergence, we also simulate the discrete model with a smaller step length of 0.001, which again leads to the same equilibrium. These results confirm that the discrete model accurately approximates the continuous dynamics and verifies the convergence of the solution as the step length decreases. Additionally, we observe that the numerical solution becomes more refined and stable with smaller step sizes, while still capturing the correct long-term behavior even for larger steps. The corresponding continuous and discrete time series are presented in Figures 2 and 3, respectively.

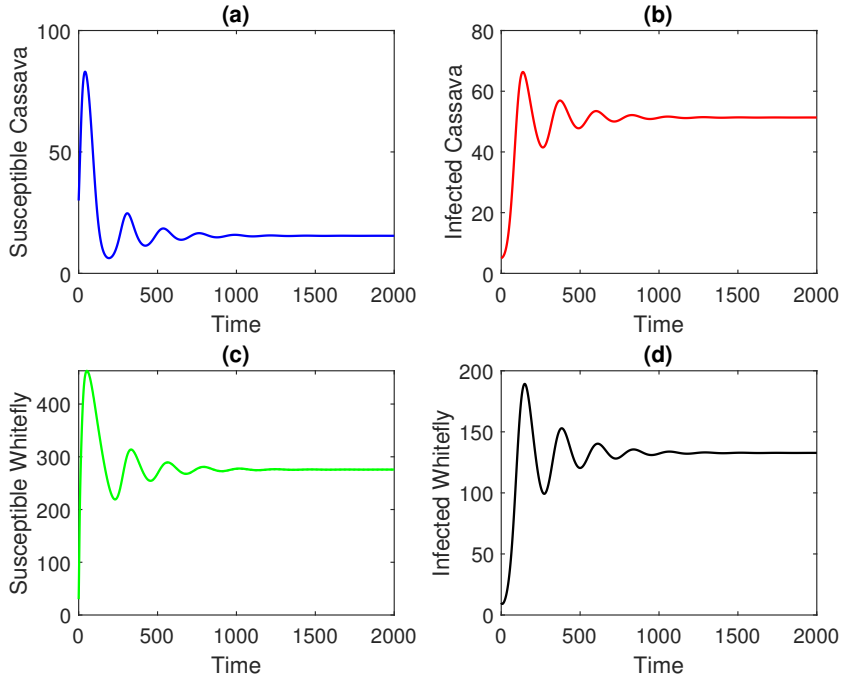

Figure 2. Time series solution of the continuous model (2.1) and parameter values are taken from Table 1.

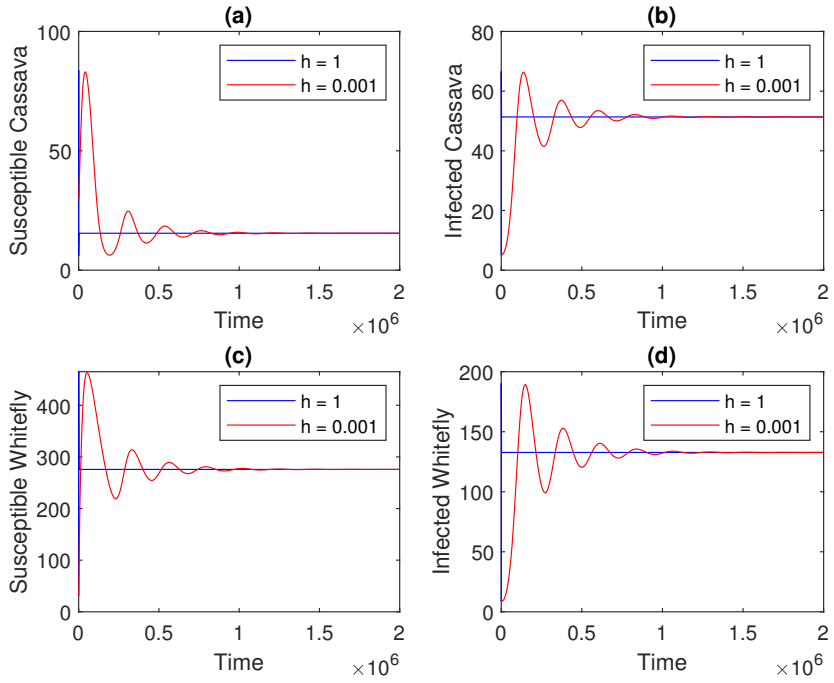

Figure 3. Time series solution of the discrete model (2.2) is generated using parameter values from Table 1, with a step size of 1 and 0.001.

The sensitivity indices of model parameters are plotted in Figure 1. The most sensitive parameters are identified using this figure as the infection rates and mortality rates. Growth rate of vector is less significant for this analysis.

9.1. Numerical stability region of fixed points

Utilizing the parameters in the Table 1, we get our three fixed points: Only the cassava plant fixed point $E_1(100.0, 0, 0, 0)$, disease-free fixed point $E_0(100.0, 0, 500.0, 0)$, and endemic fixed point $E^*(18.32, 52.84, 232.89, 115.36)$.

The stability region of fixed points is essential to study the behavior of dynamical systems. The stability region determines whether small perturbations will decay or grow. If a fixed point is stable, the system will return to it after small disturbances, ensuring predictable and controlled behavior. On the other hand, if the fixed point is unstable, even minor deviations can lead to significant divergences, potentially causing the system to become unpredictable. Here, we illustrate the stability region of our fixed points. Sobol's sensitivity analysis indicates that λ, β, a, m, and μ are the most influential parameters. However, since m and μ represent death rates, we intentionally exclude them and focus on the stability region for λ, β, and a.

We analyze the stability region for the disease-free fixed point by considering two parameter combinations: (λ, β) and (λ, a). For (λ, β), we systematically vary λ from 0 to 0.005 in very small increments, while β ranges from 0 to 0.0005. Similarly, for (λ, a), we vary λ within the same range and adjust a from 0 to 50. Figure 4 clearly illustrates these stability regions, where the blue area represents stability, while the rest of the region is unstable for the disease-free fixed point.

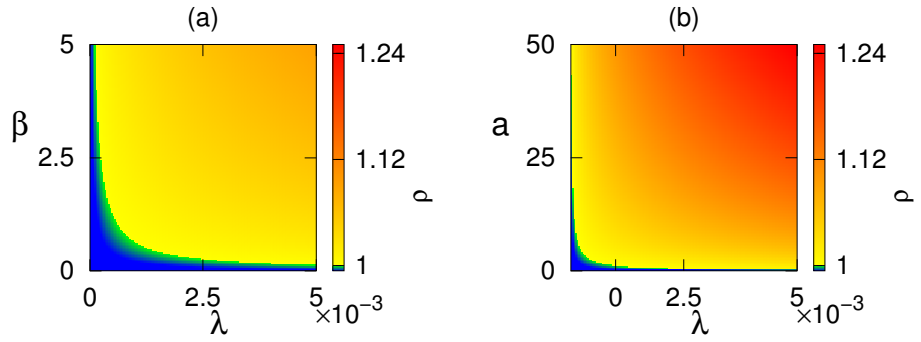

Figure 4. Stability region of the disease-free fixed point: (a) in λ-β and (b) in λ-a parameter planes and color code denotes the value of eigenvalue ρ.

Next, we illustrate the stability region of the endemic fixed point. Similarly to our previous analysis, we vary the parameters within the same range to determine the stability region of the endemic fixed point. Figure 5 illustrates the stability regions of the system across two parameter planes: (a) the $\lambda - \beta$ plane, and (b) the λ-a plane. In this figure, the blue region represents the stability region of the endemic equilibrium, while the white region corresponds to an unbounded regime for the proposed system. The remaining portion of the parameter space signifies an unstable region for the endemic fixed point. Additionally, the figure highlights that the critical value of λ for the occurrence of a Neimark-Sacker bifurcation is influenced by both the maximum abundance rate of the vector population, a, and the transmission parameter, β. In particular, when the values of either a or β are relatively low, a larger λ is necessary for the Neimark-Sacker bifurcation to generate periodic solutions, and the opposite is also true.

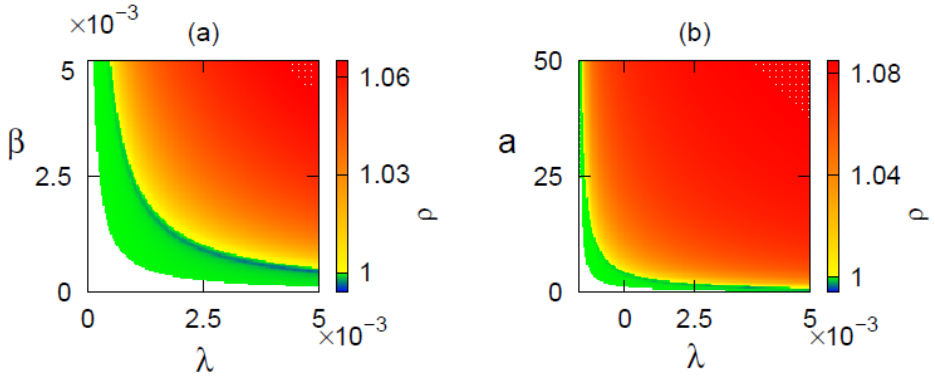

Figure 5. Stability region of the endemic fixed point: (a) in λ-β, and (b) in λ-a parameter planes and color code denote the value of eigenvalue ρ.

9.2. Bifurcations

In this subsection, we numerically verify the conditions for bifurcations of our proposed system (2.2). This verification helps detect critical parameter values where system behavior changes, validates analytical results, and aids in refining models for real-world applications. In the abovementioned Theorem 3, we proposed a condition for Neimark-Sacker bifurcation. Now, we will verify the

Neimark-Sacker bifurcation conditions for the parameters. Our proposed system exhibits Neimark-Sacker bifurcation with respect to the parameters λ, β, and a. So, we will verify Neimark-Sacker bifurcation utilizing the Theorem 3 for these parameters.

For λ:

The proposed system exhibits Neimark-Sacker bifurcation and transcritical bifurcation at $\lambda \approx 0.0004856$ and $\lambda \approx 0.0000202$, respectively. The corresponding bifurcation diagram for our system (2.2) for λ is presented in Figure 6. First, we verify the transcritical bifurcation. To verify transcritical, we take $\lambda = 0.00002$. At $\lambda = 0.00002$, the endemic point $E^*(18.32, 52.84, 232.89, 115.36)$ is unstable with eigenvalues are: 0.5223869383, 0.9497877376, 0.9963608702, 1.003026882, which indicates that all eigenvalues are not modulus less than 1. However, the disease-free fixed point $E_0(100.0, 0, 500.0, 0)$ is stable with eigenvalues: 0.5, 0.9, 0.9584817155, 0.9995182845, which indicates that all eigenvalues are less than 1. Similarly, we can obtain that after the transcritical bifurcation point, the endemic point $E^*(18.32, 52.84, 232.89, 115.36)$ is stable, and the disease-free fixed point $E_0(100.0, 0, 500.0, 0)$ is unstable.

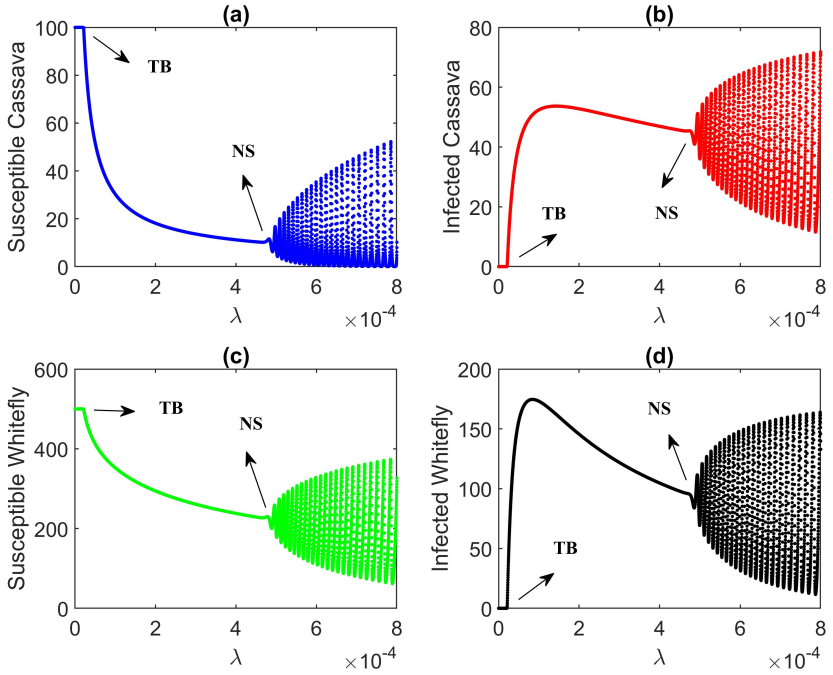

Figure 6. Neimark-Sacker (NS) bifurcation diagram of our system with respect to the parameter λ and other parameters as given in Table 1.

Second, we verify the Neimark-Sacker bifurcation at $\lambda \approx 0.0004856$. The corresponding endemic point is $E(9.91, 44.69, 223.15, 93.33)$. The characteristic equation at $E(9.91, 44.69, 223.15, 93.33)$ of the Jacobian matrix is:

$$\rho^4 - 3.275577427\rho^3 + 3.871298114\rho^2 - 1.915076641\rho + 0.319392129 = 0,$$

$\Delta_1^+(\lambda) = 1.3194 > 0$, $\Delta_1^-(\lambda) = 0.6806 > 0$, $\Delta_3^-(\lambda) \approx 0$, $\Delta_3^+(\lambda) = 0.1511 > 0$, $P_\lambda(1) = 0.000036176 > 0$, $(-1)^4 P_\lambda(-1) = 10.3813 > 0$.

All the requisite conditions for Neimark-Sacker bifurcation occur near the sole positive equilibrium point $E(9.91, 44.69, 223.15, 93.33)$. Therefore, following Theorem 3, all four populations undergo Neimark-Sacker bifurcation at the critical parameter value $\lambda \approx 0.0004856$.

For β:

The proposed system exhibits Neimark-Sacker and transcritical bifurcations similar to λ at $\beta \approx 0.000597$ and $\beta \approx 0.0000242$, respectively. Figure 7 depicted this scenario. We adopt the opposite approach in the previous analysis of the parameter λ to verify the transcritical bifurcation. So, we choose $\beta = 0.00003$, and the endemic equilibrium $E^*(18.32, 52.84, 232.89, 115.36)$ is stable, with eigenvalues: 0.5213219503, 0.9633166972, $0.987328253 - 0.02325474055i$, $0.987328253 + 0.02325474055i$ are less than 1. Conversely, the disease-free equilibrium $E_0(100.0, 0, 500.0, 0)$ is stable, as its eigenvalues are: $0.5, 0.9, 0.9567289425$, and 1.001271057. The equilibrium E_0 is unstable since at least one eigenvalue has a modulus greater than 1. Additionally, before the transcritical bifurcation point, stability reverses: the endemic equilibrium $E^*(18.32, 52.84, 232.89, 115.36)$ loses stability, whereas the disease-free equilibrium $E_0(100.0, 0, 500.0, 0)$ becomes stable.

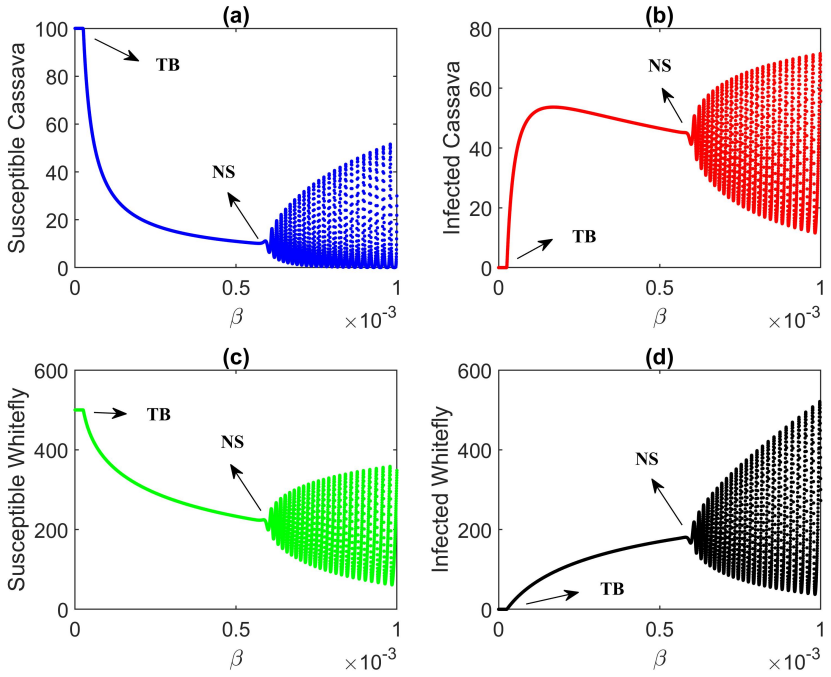

Figure 7. Neimark-Sacker bifurcation diagram of our system with respect to the parameter β and other parameters as given in Table 1.

Now, to verify Neimark-Sacker bifurcation, the condition given in Theorem 3 must be satisfied. The point $E(9.77, 44.60, 219.36, 182.51)$ is the corresponding endemic point. The characteristic equation at $E(9.77, 44.60, 219.36, 182.51)$ of the Jacobian matrix is:

$$\rho^4 - 2.943363625\rho^3 + 2.909018638\rho^2 - 0.9865333294\rho + 0.02094095539 = 0,$$

and $\Delta_1^+(\beta) = 1.0209 > 0$, $\Delta_1^-(\beta) = 0.9791 > 0$, $\Delta_3^-(\beta) \approx 0$, $\Delta_3^+(\beta) = 0.2935 > 0$, $P_\beta(1) = 0.000062640 > 0$, $(-1)^4 P_\beta(-1) = 7.8599 > 0$.

Thus, all the necessary conditions for a Neimark-Sacker bifurcation are fulfilled near the unique positive equilibrium point $E(9.77, 44.60, 219.36, 182.51)$. Consequently, as established in Theorem 3, all four populations undergo a Neimark-Sacker bifurcation at the critical bifurcation parameter value $\beta \approx 0.000597$. The corresponding bifurcation diagram for our system (2.2) with respect to λ is depicted in Figure 7.

For a:

The proposed system exhibits Neimark-Sacker bifurcation at $a \approx 8.676$. According to the theorem 3, the condition given in this theorem must be satisfied. The point $E(9.94, 45.24, 424.47, 180.39)$ is the corresponding endemic point. The characteristic equation at $E(9.94, 45.24, 424.47, 180.39)$ of the Jacobian matrix is:

$$\rho^4 - 3.170764152\rho^3 + 3.564111261\rho^2 - 1.615002924\rho + 0.2216964434 = 0,$$

and $\Delta_1^+(a) = 1.2217 > 0$, $\Delta_1^-(a) = 0.7783 > 0$, $\Delta_3^-(a) \approx 0$, $\Delta_3^+(a) = 0.1857 > 0$, $P_a(1) = 0.000040628 > 0$, $(-1)^4 P_a(-1) = 9.5716 > 0$.

Hence, all the necessary conditions for Neimark-Sacker bifurcation are met in the vicinity of the unique positive equilibrium point $E(9.94, 45.24, 424.47, 180.39)$. Consequently, as stated in Theorem 3, all four populations experience Neimark–Sacker bifurcation at the critical bifurcation parameter value $a \approx 8.676$. The corresponding bifurcation diagram for our system (2.2) for a is presented in Figure 8.

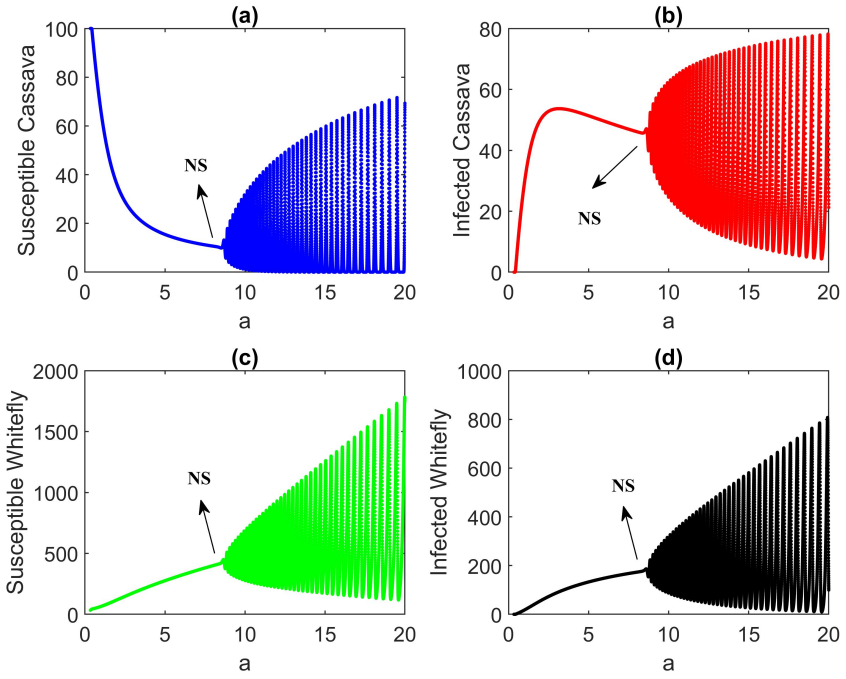

Figure 8. Neimark-Sacker (NS) bifurcation diagram of our system with respect to the parameter a and other parameters as given in Table 1.

9.3. Advantages

The discrete modeling framework adopted in this study offers several compelling advantages, especially when applied to the epidemiology of cassava mosaic disease. First and foremost, discrete-time models naturally align with the intervals at which real-world data on plant diseases are typically collected, often on a weekly, monthly, or seasonal basis rather than continuously. This congruence minimizes the errors and improves model accuracy and relevance for field-based applications. Mosaic disease in cassava is heavily influenced by seasonal agricultural practices and environmental conditions, such as planting and harvesting cycles. A discrete framework is often easier to implement and interpret, especially for stakeholders such as agricultural officers, disease monitoring teams, and policy-makers who may not have extensive mathematical training. So, a step-by-step progression of a discrete model makes it a more accessible and transparent tool for planning and decision-making. The previous studies [20, 29] are based on a continuous setup, and they discussed qualitative and quantitative dynamics of the cassava mosaic disease. Their results show an oscillatory behavior of the system. Similarly, our discrete model shows a strong alignment with the oscillatory behavior of the system through the Neimark-Sacker bifurcation. Thus, aligning with continuous setup in qualitative and quantitative trends. This cross-validation demonstrates that discrete models can preserve the core epidemiological insights of continuous models while offering greater flexibility and practicality. In summary, the discrete model not only simplifies application and captures key real-world features such as seasonality, but it also enhances our ability to understand and manage the intricate dynamics of cassava mosaic disease outbreaks, making it a valuable tool for researchers and practitioners alike.

10. Discussion and conclusions

In this study, we have developed a discrete-time mathematical model to describe the interaction dynamics between cassava plants and the whitefly vector population, which plays a crucial role in the spread of cassava mosaic disease. To facilitate the analysis of disease dynamics, we derive the discrete-time model from an existing continuous-time framework. This transformation allows for a more comprehensive exploration of disease propagation patterns under different conditions.

We conduct a rigorous analytical study of the model, ensuring the solutions remain nonnegative and bounded over time. Additionally, we determine the basic reproduction number $\mathcal{R}_0$ and investigate the disease-free equilibrium (DFE) stability. The system's fixed points are identified, and their stability properties are analyzed. Furthermore, we explore the occurrence of Neimark-Sacker bifurcation, which depends on key model parameters, highlighting the complex dynamical behavior that emerges under varying infection rates. A sensitivity analysis using Sobol indices is performed to assess the robustness of the model, identifying the most influential parameters governing disease transmission. Our findings establish that the DFE remains stable when $\mathcal{R}_0 < 1$, while an endemic equilibrium emerges when $\mathcal{R}_0 > 1$. Notably, when the basic reproduction number exceeds unity, the system exhibits stable coexistence of all four populations for low infection rates. However, as the infection rate increases, the system undergoes a Neimark-Sacker bifurcation, leading to periodic oscillations via limit cycles. Stability regions in various parameter planes indicate that multiple interacting parameters influence the critical bifurcation threshold. Formulating a discrete-time model is particularly significant, as bridging the results between discrete and continuous models presents inherent challenges. Through both analytical and numerical investigations, we demonstrate that the discrete model effectively replicates

the key dynamical features observed in the corresponding continuous-time models presented in [20,29]. This study offers several key innovations that advance the understanding of cassava mosaic disease dynamics. By employing a discrete-time modeling framework, it bridges the gap between theoretical epidemiology and practical disease management, capturing both seasonal variations and realistic data collection intervals. The validation against continuous models not only confirms the robustness of the discrete approach but also highlights its versatility in modeling complex outbreak behaviors.

In conclusion, the proposed discrete-time model successfully captures the intricate dynamics of cassava mosaic disease. The analytical techniques employed, including stability analysis, bifurcation analysis, and sensitivity analysis, provide valuable insights into the behavior of a four-dimensional discrete-time epidemiological system. These findings contribute to a deeper understanding of disease transmission mechanisms and may inform effective disease management strategies.

While the discrete modeling setup captures key dynamics and seasonal effects, it does not account for time delays or incorporate optimal control strategies. These elements, often included in continuous models [19], could further enhance the model's applicability and realism in future extensions.

Author contributions

Selim Reja: Conceptualization, methodology, writing original draft preparation, supervision, writing formal analysis, validation, software, visualization; Fahad Al Basir: Conceptualization, methodology, writing original draft preparation, supervision; Khalid Aldawsari: Methodology, validation, software. All authors have read and agreed to publish the manuscript.

Use of Generative-AI tools declaration

The authors declare they have not used Artificial Intelligence (AI) tools in the creation of this article.

Acknowledgments

This study is supported via funding from Prince Sattam bin Abdulaziz University project number (PSAU/2025/R/1447).

Conflict of interest

The authors declare no conflict of interest.

References

1. M. Chapwanya, Y. Dumont, Application of mathematical epidemiology to crop vector-borne diseases: The cassava mosaic virus disease case, In: *Infectious Diseases and our planet*, Cham: Springer, 2021, 57–95. https://doi.org/10.1007/978-3-030-50826-5_4
2. R. Bhaargavi, T. K. S. Latha, T. Makeshkumar, S. Harish, Cassava mosaic disease: strategies for recovery and sustainable management, *Australasian Plant Pathol.*, **54** (2025), 1–12. https://doi.org/10.1007/s13313-024-01014-1

3. J. Legg, S. Winter, Cassava mosaic viruses (Geminiviridae), *Encyclopedia of Virology (Fourth Edition)*, **3** (2021), 301–312. https://doi.org/10.1016/B978-0-12-809633-8.21523-9

4. O. Chase, I. Ferriol, J. J. López-Moya, Control of plant pathogenic viruses through interference with insect transmission, In: *Plant virus-host interaction*, 2 Eds., New Yourk: Academic Press, 2021, 359–381. https://doi.org/10.1016/B978-0-12-821629-3.00019-1

5. K. M. G. Chanchala, Management of disease-transmitting insect vectors, In: *Plant diseases and their management*, New York: Apple Academic Press, 2024, 191–220. https://doi.org/10.1201/9781032722856-7

6. D. Fargette, M. J. Jeger, C. Fauquet, L. D. C. Fishpool, Analysis of temporal disease progress of African cassava mosaic virus, *Phytopathology*, **84** (1994), 89–91. http://doi.org/10.1094/Phyto-84-91

7. E. W. Kitajima, An annotated list of plant viruses and viroids described in Brazil (1926–2018), *Biota Neotrop.*, **20** (2020), v20n2. https://doi.org/10.1590/1676-0611-BN-2019-0932

8. A. G. Power, Virus spread and vector dynamics in genetically diverse plant populations, *Ecology*, **72** (1991), 232–241. https://doi.org/10.2307/1938917

9. J. Navas-Castillo, E. Fiallo-Olivé, S. Sánchez-Campos, Emerging virus diseases transmitted by whiteflies, *Annu. Rev. Phytopathol.*, **49** (2011), 219–248. https://doi.org/10.1146/annurev-phyto-072910-095235

10. M. Abubakar, B. Koul, K. Chandrashekar, A. Raut, D. Yadav, Whitefly (Bemisia tabaci) management (WFM) strategies for sustainable agriculture: A review, *Agriculture*, **12** (2022), 1317. https://doi.org/10.3390/agriculture12091317

11. J. Bird, K. Maramorosch, Viruses and virus diseases associated with whiteflies, *Adv. Virus Res.*, **22** (1978), 55–110. https://doi.org/10.1016/S0065-3527(08)60772-1

12. F. Al Basir, K. B. Blyuss, E. Venturino, Stability and bifurcation analysis of a multi-delay model for mosaic disease transmission, *AIMS Mathematics*, **8** (2023), 24545–24567. https://doi.org/10.3934/math.20231252

13. M. Chapwanya, Y. Dumont, Application of mathematical epidemiology to crop vector-borne diseases: The cassava mosaic virus disease case, In: *Infectious diseases and our planet*, Cham: Springer, 2021, 57–95. https://doi.org/10.1007/978-3-030-50826-5_4

14. F. D. Magoyo, J. I. Irunde, D. Kuznetsov, Modeling the dynamics and transmission of cassava mosaic disease in Tanzania, *Commun. Math. Biol. Neurosci.*, **2019** (2019), 4. https://doi.org/10.28919/cmbn/3819

15. M. J. Jeger, J. Holt, F. Van Den Bosch, L. V. Madden, Epidemiology of insect-transmitted plant viruses: modelling disease dynamics and control interventions, *Physiol. Entomol.*, **29** (2004), 291–304. https://doi.org/10.1111/j.0307-6962.2004.00394.x

16. S. Maity, P. S. Mandal, A comparison of deterministic and stochastic plant-vector-virus models based on probability of disease extinction and outbreak, *Bull. Math. Biol.*, **84** (2022), 41. https://doi.org/10.1007/s11538-022-01001-x

17. C. F. McQuaid, F. van den Bosch, A. Szyniszewska, T. Alicai, A. Pariyo, P. C. Chikoti, et al., Spatial dynamics and control of a crop pathogen with mixed-mode transmission. *PLoS Comput. Biol.*, **13** (2017), e1005654. https://doi.org/10.1371/journal.pcbi.1005654

18. Z. Lawrence, D. I. Wallace, The spatiotemporal dynamics of African cassava mosaic disease, In: BIOMAT 2010: International symposium on mathematical and computational biology, Singapore: World Scientific, 2011, 236–255. https://doi.org/10.1142/9789814343435_0016

19. F. Al Basir, P. K. Roy, Dynamics of mosaic disease with roguing and delay in Jatropha curcas plantations, *J. Appl. Math. Comput.*, **58** (2018), 1–31. https://doi.org/10.1007/s12190-017-1131-2

20. F. Al-Basir, P. K. Roy, S. Ray, Impact of roguing and insecticide spraying on mosaic disease in Jatropha curcas, *Control Cybern.*, **46** (2017), 325–344.

21. F. Al Basir, Y. N. Kyrychko, K. B. Blyuss, S. Ray, Effects of vector maturation time on the dynamics of cassava mosaic disease. *Bull. Math. Biol.*, **83** (2021), 87. https://doi.org/10.1007/s11538-021-00921-4

22. J. E. Franke, A. A. Yakubu, Disease-induced mortality in density-dependent discrete-time SIS epidemic models, *J. Math. Biol.*, **57** (2008), 755–790. https://doi.org/10.1007/s00285-008-0188-9

23. C. Castillo-Chavez, A. A. Yakubu, Discrete-time S-I-S models with complex dynamics, *Nonlinear Anal.-Theor.*, **47** (2001), 4753–4762. https://doi.org/10.1016/S0362-546X(01)00587-9

24. M. Sekiguchi, E. Ishiwata, Global dynamics of a discretized SIRS epidemic model with time delay, *J. Math. Anal. Appl.*, **371** (2010), 195–202. https://doi.org/10.1016/j.jmaa.2010.05.007

25. L. J. S. Allen, A. M. Burgin, Comparison of deterministic and stochastic SIS and SIR models in discrete time, *Math. Biosci.*, **163** (2000), 1–33. https://doi.org/10.1016/S0025-5564(99)00047-4

26. J. Q. Li, Z. E. Ma, F. Brauer, Global analysis of discrete-time SI and SIS epidemic models, *Math. Biosci. Eng.*, **4** (2007), 699–710. https://doi.org/10.3934/mbe.2007.4.699

27. Z. Y. Hu, Z. D. Teng, H. J. Jiang, Stability analysis in a class of discrete SIRS epidemic models, *Nonlinear Anal.-Real*, **13** (2012), 2017–2033. https://doi.org/10.1016/j.nonrwa.2011.12.024

28. L. J. Chen, L. J. Chen, Permanence of a discrete periodic Volterra model with mutual interference, *Discrete Dyn. Nat. Soc.*, **2009** (2009), 205481. https://doi.org/10.1155/2009/205481

29. J. Holt, M. J. Jeger, J. M. Thresh, G. W. Otim-Nape, An epidemilogical model incorporating vector population dynamics applied to African cassava mosaic virus disease, *J. Appl. Ecol.*, **34** (1997), 793-806. https://doi.org/10.2307/2404924

30. J. Chowdhury, F. Al Basir, A. Mukherjee, P. K. Roy, A theta logistic model for the dynamics of whitefly borne mosaic disease in Cassava: impact of roguing and insecticide spraying, *J. Appl. Math. Comput.*, **71** (2025), 4897–4914. https://doi.org/10.1007/s12190-025-02419-x

31. A. Columbu, R. D. Fuentes, S. Frassu, Uniform-in-time boundedness in a class of local and nonlocal nonlinear attraction-repulsion chemotaxis models with logistics, *Nonlinear Anal.-Real*, **79** (2024), 104135. https://doi.org/10.1016/j.nonrwa.2024.104135

32. T. X. Li, D. Acosta-Soba, A. Columbu, G. Viglialoro, Dissipative gradient nonlinearities prevent δ-formations in local and nonlocal attraction-repulsion chemotaxis models, *Stud. Appl. Math.*, **154** (2025), e70018. https://doi.org/10.1111/sapm.70018

33. S. Gnanasekaran, A. Columbu, R. D. Fuentes, N. Nithyadevi, Global existence and lower bounds in a class of tumor-immune cell interactions chemotaxis systems, *Discrete Cont. Dyn.-S*, **18** (2025), 1636–1659. https://doi.org/10.3934/dcdss.2024174

34. H. Christopher Frey, S. R. Patil, Identification and review of sensitivity analysis methods, *Risk Anal.*, **22** (2002), 553–578. https://doi.org/10.1111/0272-4332.00039

35. S. Sangsawang, U. W. Humphries, A. Khan, P. Pongsumpun, Sensitivity analysis of cassava mosaic disease with saturation incidence rate model, *AIMS Mathematics*, **8** (2023), 6233–6254. https://doi.org/10.3934/math.2023315

36. G. Izzo, Y. Muroya, A. Vecchio, A general discrete time model of population dynamics in the presence of an infection, *Discrete Dyn. Nat. Soc.*, **2009** (2009), 143019. https://doi.org/10.1155/2009/143019

37. J. M. Heffernan, R. J. Smith, L. M. Wahl, Perspectives on the basic reproductive ratio, *J. R. Soc. Interface*, **2** (2005), 281–293. https://doi.org/10.1098/rsif.2005.0042

38. P. Van den Driessche, J. Watmough, Reproduction numbers and sub-threshold endemic equilibria for compartmental models of disease transmission, *Math. Biosci.*, **180** (2002), 29–48. https://doi.org/10.1016/S0025-5564(02)00108-6

39. S. Reja, S. Ghosh, I. Ghosh, A. Paul, S. Bhattacharya, Investigation and control strategy for canine distemper disease on endangered wild dog species: A model-based approach, *SN Appl. Sci.*, **4** (2022), 176. https://doi.org/10.1007/s42452-022-05053-5

40. M. C. M. De Jong, O. Diekmann, J. A. P. Heesterbeek, The computation of R_0 for discrete-time epidemic models with dynamic heterogeneity, *Math. Biosci.*, **119** (1994), 97–114. https://doi.org/10.1016/0025-5564(94)90006-X

41. L. J. S. Allen, P. van den Driessche, The basic reproduction number in some discrete-time epidemic models, *J. Differ. Equ. Appl.*, **14** (2008), 1127–1147. https://doi.org/10.1080/10236190802332308

42. K. Ogata, *Discrete-time control systems*, Prentice-Hall. 1995.

43. M. Benidir, On the root distribution of general polynomials with respect to the unit circle, *Signal Process.*, **53** (1996), 75–82. https://doi.org/10.1016/0165-1684(96)00077-1

44. G. L. Wen, Criterion to identify Hopf bifurcations in maps of arbitrary dimension, *Phys. Rev. E*, **72** (2005), 026201. https://doi.org/10.1103/PhysRevE.72.026201

45. U. Saeed, I. Ali, Q. Din, Neimark–Sacker bifurcation and chaos control in discrete-time predator-prey model with parasites, *Nonlinear Dyn.*, **94** (2018), 2527–2536. https://doi.org/10.1007/s11071-018-4507-4

46. L. Rimbaud, C. Bruchou, S. Dallot, D. R. J. Pleydell, E. Jacquot, S. Soubeyrand, et al., Using sensitivity analysis to identify key factors for the propagation of a plant epidemic, *R. Soc. Open Sci.*, **5** (2018), 171435. https://doi.org/10.1098/rsos.171435

47. J. Y. Wu, R. Dhingra, M. Gambhir, J. V. Remais, Sensitivity analysis of infectious disease models: methods, advances and their application, *J. R. Soc. Interface*, **10** (2013), 20121018. https://doi.org/10.1098/rsif.2012.1018

48. S. Marino, I. B. Hogue, C. J. Ray, D. E. Kirschner, A methodology for performing global uncertainty and sensitivity analysis in systems biology, *J. Theor. Biol.*, **254** (2008), 178–196. https://doi.org/10.1016/j.jtbi.2008.04.011

49. I. Y. M. Sobol, On sensitivity estimation for nonlinear mathematical models, *Matematicheskoe Modelirovanie*, **2** (1990), 112–118.

50. I. M. Sobol, Global sensitivity indices for nonlinear mathematical models and their Monte Carlo estimates, *Math. Comput. Simulat.*, **55** (2001), 271–280. https://doi.org/10.1016/S0378-4754(00)00270-6

AIMS Press